scientific reports

Check for updates

OPEN

Computational sensitivity evaluation of ultrasound neuromodulation resolution to brain tissue sound speed with robust beamforming

Boqiang Fan[1]✉, Wayne Goodman[1,2], Sameer A. Sheth[1,3], Richard R. Bouchard[4] & Behnaam Aazhang[1]

Low-intensity focused ultrasound (LIFU) neuromodulation requires precise targeting and high resolution enabled by phased array transducers and beamforming. However, focusing optimization usually relies on phantom measurements or simulations with inaccurate acoustic properties to degrade neuromodulation resolution. Therefore, this work analyzes the sensitivity of neuromodulation resolution, measured by off-target activation area (OTAA), to brain tissue sound speed. A Robust Optimal Resolution (ROR) beamforming method is proposed to minimize the worst-case OTAA with restricted sound speed inaccuracy and propagation information estimated with deviated sound speed. The propagation estimation model utilizes equivalent source method (ESM) to map sound field between different acoustic parameter sets. Simulation in a human head model validates the effectiveness of the proposed propagation estimation model, and shows that ROR beamforming method can significantly reduce the worst-case OTAA compared to benchmark methods by 78.0% on average and up to 90.0%, improving the robustness of stimulation and addressing the sensitivity issue. This allows reliable high-resolution neuromodulation in potential clinical applications with reduced invasive acquisition of propagation measurements for focusing optimization.

As a novel technology, low-intensity focused ultrasound (LIFU) neuromodulation has the potential to be applied to treating neuropsychiatric disorders in the future[1]. As is demonstrated in previous research, the responses of neural circuits to ultrasonic waves significantly depend on the accuracy of targeting during LIFU stimulation[2–5]. Therefore, a high neuromodulation resolution is expected for future LIFU applications to limit the unintended neuromodulation side effect while ensuring successful neuron activation in the target brain region. Such required neuromodulation resolution can be measured by the Off-Target Activation Area (OTAA) metric as is defined in the literature[6,7], and is achievable with ultrasound focusing solutions.

Ultrasound focusing design and performance has been shown to strongly depend on tissue acoustic properties. Accurate focusing requires the waves from the transducer to be phase-aligned at the target location, and a corresponding transducer design is determined by the acoustic propagation in tissues. However, the propagation is usually hard to measure *in vivo* due to the high invasiveness[8]. Instead, many investigators can only design focusing methods and validate the ultrasound focusing performance via independent phantom experiments or simulations[7,9–11]. As a result, the actual focusing resolution relies on the accuracy of computational or phantom model used for design or validation. A degradation of neuromodulation resolution is expected when inaccuracy exists, e.g., inaccurate tissue acoustic parameters used for simulations[12]. Unfortunately, these parameters for brain tissues can also be hard to accurately acquire *in vivo*, allowing such degradations in real-world applications.

Given potentially random error in the tissue acoustic parameters used in computational or phantom model, the dependence of transcranial ultrasound focusing performance (especially in the worst case) on such inaccuracy, i.e., sensitivity, is a very important metric to evaluate the robustness and reliability of ultrasound neuromodulation. Literature[12–14] has shown via simulated transcranial stimulations that the ultrasound focusing

[1]Department of Electrical and Computer Engineering, Rice University, Houston, TX 77005, USA. [2]Department of Psychiatry and Behavioral Science, Baylor College of Medicine, Houston, TX 77030, USA. [3]Department of Neurosurgery, Baylor College of Medicine, Houston, TX 77030, USA. [4]Department of Imaging Physics, University of Texas MD Anderson Cancer Center, Houston, TX 77030, USA. ✉email: Boqiang.Fan@rice.edu

performance, like the peak pressure and the focus location, can be sensitive to the variance of the skull acoustic properties (e.g., sound speed, attenuation, etc.). Although it has generally been acknowledged that the acoustic properties of the cranial bones can affect ultrasound focusing, there is no consensus on whether it is also affected by the acoustic properties of brain tissues (such as grey and white matter). Some optimistic results[13] show that the acoustic properties of brain tissues have small influences on the focusing performance in transcranial stimulation setup. However, opposing conclusions have been drawn in some other works[15], in which a simplified layered tissue model has been investigated and shown that the focal area can be substantially influenced by the change of brain tissue sound speed. Besides, the sensitivity of focusing performance to brain tissue acoustic properties can also be more significant for an intracranially embedded transducer[16] due to a reduction of skull attenuation, which is a promising solution for real-time treatment but has not been well investigated yet.

Previous sensitivity analyses are primarily focused on the ultrasound beam profiles, while the dependence of brain neuron activities on the inaccuracy of acoustic parameters in brain tissues remains unclear[6]. Therefore in this work, a framework to analyze the sensitivity of the neuromodulation resolution to the sound speed in brain tissues has been proposed, which can be generalized to evaluate the sensitivity to other tissue parameters in future work. The multi-scale optimized neuronal intramembrane cavitation (SONIC) model is applied in this work to model individual neuronal activities with ultrasound stimulation[17]. The sensitivity of ultrasound neuromodulation has been confirmed in our simulations given conventional ultrasound focusing methods, and a Robust Optimal Resolution (ROR) beamforming algorithm has been proposed to mitigate such sensitivity and provide high-resolution LIFU neuromodulation. The ROR beamforming method minimizes the worst-case OTAA for all potential sound speed values, relying on an inference of intracranial propagation with arbitrary sound speed values given limited reference measurements. The proposed ROR beamforming methods are computationally evaluated in a 2-D human head model[18] with intracranial phased array transducers, and simulations show that the ROR beamforming scheme can successfully solve the sensitivity problem by robustly providing high-resolution stimulation to the target brain region.

Methods

Computational modeling of neuromodulation resolution

Experiments and simulations in literature have shown that the neuromodulation effect is highly target-specific i.e., stimulating different target points or off-target tissues can result in unexpected neuromodulation effects according to literature results[2–5]. Therefore, high neuromodulation resolution is necessary for practical usage of this technology. Previous works have shown that the neuromodulation resolution can be computationally modeled by OTAA[7], which computes the ultrasound energy distribution in brain tissues and the corresponding excitatory neuron spiking patterns given ultrasound stimulation based on SONIC model[17]. Therefore, this work also utilizes OTAA as the metric of neuromodulation resolution, and similarly assumes regular spiking neurons in brain tissues as in previous work[7]. Other neuron types and factors (e.g., anesthesia state) will be considered in future works.

Framework for analyzing sensitivity of neuromodulation resolution

High-resolution neuromodulation requires ultrasound focusing, which relies on beamforming when transducer arrays are used for stimulation. The optimization of beam further relies on accurate knowledge of wave propagation or acoustic properties such as sound speeds. Inaccuracy in the knowledge of sound speeds can diminish the focusing effect and degrade the neuromodulation resolution. The impact of such inaccuracy on neuromodulation resolution, defined as the sensitivity, is hence an important metric of reliability for this emerging technology. This work proposes a general framework to computationally analyze the sensitivity of neuromodulation resolution to the sound speed in brain tissues, as is shown in Fig. 1. With a human head model shown in Fig. 1 (a), the k-Wave toolbox[19] can integrate the driving signals of the ultrasound transducer in Fig. 1 (b) and simulate the ultrasound beam map in brain tissue regions, as is shown in Fig. 1 (c). For sensitivity analysis, different tissue sound speed values, e.g., from c_1 to c_n, need to be assumed in k-Wave simulations to generate corresponding beam maps and demonstrate the impact of sound speed inaccuracy. Note that each c_n represents a set of sound speed values for different brain tissues in nth k-Wave simulation. Given the ultrasound energy distribution in Fig. 1 (c), SONIC model can be used to compute the excitatory neuron spiking pattern in each brain region and generate the neuron spike count map with different sound speed values from c_1 to c_n in Fig. 1 (d). Further sensitivity analysis, e.g., best-case / worst-case resolution, is conducted using the generated neuron spike maps.

This work assumes stimulation using continuous ultrasound waves at frequency $f = 250$ kHz[2,20]. Although pulsed wave stimulation and some other frequencies (e.g., 500 kHz) might be more common in literature[20,21], using continuous wave at lower frequency could significantly reduce the computational complexity for initial evaluation. Higher frequencies and pulsed wave stimulation will be tested in the future work. An example of simulated excitatory neuron spike pattern using SONIC model at f is shown in Fig. 2 (a). Continuous stimulation is exerted on a single neuron since time $t = 0$, and the stimulated neuron starts continuous spiking with a delay. Fig. 2 (b) shows a relationship between neuronal firing rate and the average intensity, in which the firing rate generally increases with the stimulation intensity. There is also an intensity threshold for neuron excitation, which can be utilized to avoid unintended neuron excitation to other brain regions during LIFU stimulation[7].

Beam focusing model with sensitivity mitigation

The driving signals of the ultrasound transducer in Fig. 1 (b) determine the ultrasound beam profile. Conventional driving signals are calculated based on the simulation / phantom measurement of ultrasound propagation, which further rely on a single set of sound speed values used by the simulator or phantom experiment. One challenge of these methods is that the focusing resolution can degrade when there are differences between the actual tissue

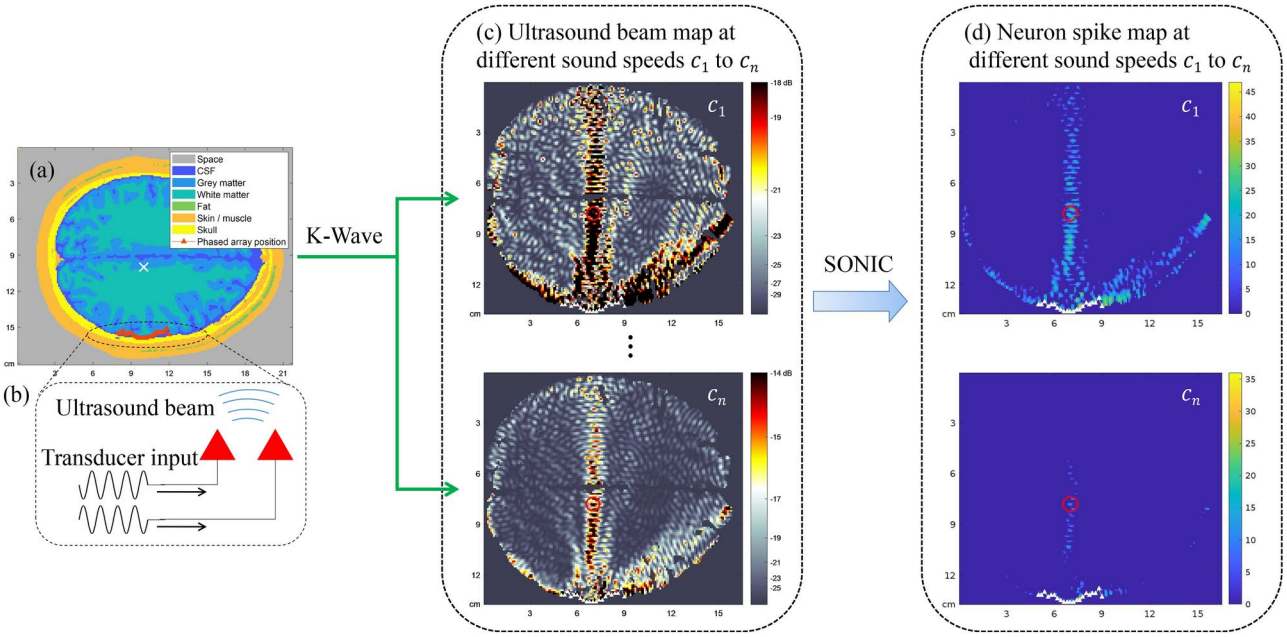

Fig. 1. The framework of sensitivity analysis for LIFU neuromodulation resolution. (**a**) A 2-D cross section of the human head model built from the imaging data[18], in which the target region is denoted by the white cross and transducer elements on the surface of brain tissues are denoted by red triangles. (**b**) Illustration of driving signals for ultrasound transducer beam. (**c**) Ultrasound beam maps simulated with k-Wave toolbox at different sound speed values from c_1 to c_n (usually sampled in a potential range of feasible values). Each c_n represents a set of sound speed values for different brain tissues in nth k-Wave simulation. (**d**) The neuron spike count map at different sound speed values from c_1 to c_n.

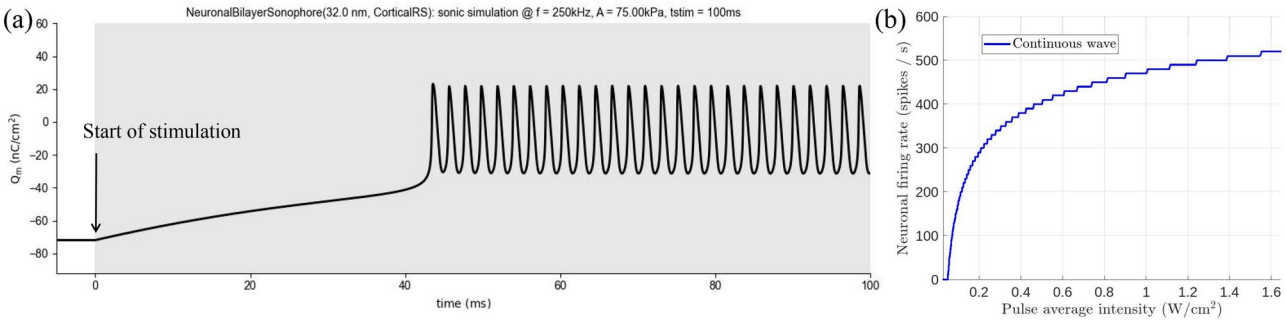

Fig. 2. Illustration of SONIC simulation results for continuous wave at $f = 250$ kHz. (**a**) An example spike pattern of a single neuron stimulated since $t = 0$ simulated with SONIC model. (**b**) The firing rate of a single neuron during 100 ms stimulation with respect to the intensity.

sound speed values of the stimulation subject and the values used. Although this challenge can be apparently addressed by using propagation information at all potential sound speed values together for beam design, the simulation / measurement cost and complexity will not be affordable. Therefore, the ROR beamforming method is proposed to achieve high neuromodulation resolution and reduce such sensitivity with limited simulation / measurement cost. The framework of ROR beam optimization is illustrated in Fig. 3. Based on the human head model and the phased array transducer, the ultrasound propagation can first be simulated with a limited set of reference sound speed values c_r using the k-Wave toolbox[19]. Then an Equivalent Source Method (ESM) can be used to infer propagation properties with any arbitrary sound speed values from the simulation results. ROR beamforming algorithm can comprehensively consider the propagation with any sound speed values, and optimize the beam profile as well as driving signals. ROR aims to minimize the worst-case OTAA to reduce the sensitivity of OTAA to the sound speed inaccuracy.

Two benchmark methods, conjugate beamforming and Constrained Optimal Resolution (COR) beamforming, whose details are introduced in the Supplementary Information, are also evaluated in this work with respect to the proposed method. Both benchmark methods only consider the beam optimization with a single set of sound speed values and fail to consider the sensitivity. Conjugate beamforming aims to maximize

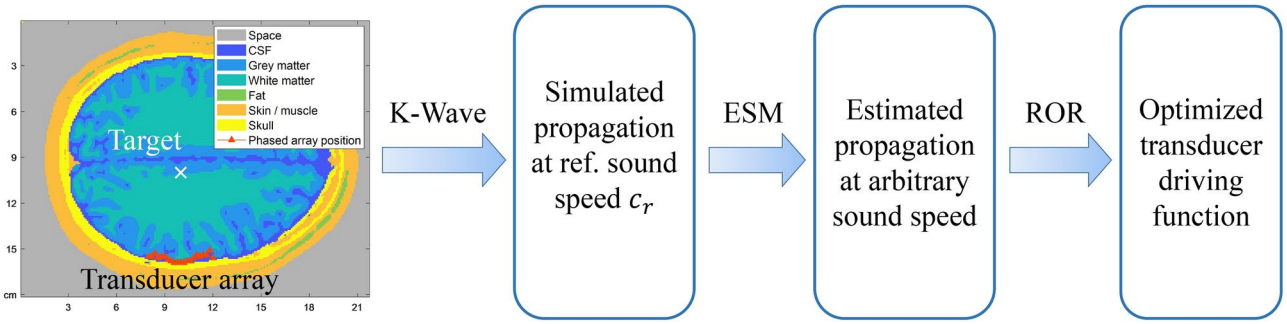

Fig. 3. The proposed ROR beam optimization framework for sensitivity mitigation. First, the ultrasound propagation from the phased array transducer to any brain region in the given human head model can be simulated with a limited set of reference sound speed values c_r using the k-Wave toolbox[19]. Next, an Equivalent Source Method (ESM) can be used to infer propagation properties with any arbitrary sound speed values $c \neq c_r$ from the propagation simulation results. Finally, ROR beamforming algorithm can optimize the beam profile as well as driving signals by comprehensively considering the propagation properties with any potential sound speed values c inferred with ESM.

the ultrasound intensity delivered to the target region, and COR beamforming aims to minimize OTAA while ensuring a successful stimulation[7].

Modeling ultrasound propagation

The ultrasound propagation in the human head model depends on tissue acoustic properties, including the density, the attenuation coefficient, and the sound speed $c(G)$ in each brain region G. However, measuring the acoustic properties of the human subject *in vivo* is highly invasive and challenging, while using empirical values[22,23] can involve inaccuracy due to individual differences that affects neuromodulation resolution. Therefore, in this work, the sensitivity of ultrasound neuromodulation resolution to the inaccuracy of brain tissue sound speeds is evaluated[12,13].

It is assumed that the actual sound speed $c(G)$ in each brain region G can be modeled as

$$c(G) = (1+\epsilon)\bar{c}(G), \ \epsilon \in [\epsilon_{min}, \epsilon_{max}]. \tag{1}$$

Here $\bar{c}(G)$ denotes a statistical sound speed value in the brain tissue at G, and ϵ denotes the deviation of the sound speed at G with respect to $\bar{c}(G)$. It is assumed that ϵ is limited in a small range $[\epsilon_{min}, \epsilon_{max}]$ (usually with $\epsilon_{min} < 0$ and $\epsilon_{max} > 0$) and can be either positive or negative. The value of $c(G)$ is unknown, whereas $\bar{c}(G)$, ϵ_{min} and ϵ_{max} can be estimated from the range of sound speed values measured in the literature. All brain regions G share the same ϵ value, including grey matter and white matter, which is an accepted assumption in the previous work[13]. Although in real-world scenarios, it is intuitive to have medium-specific / location-specific deviation, there is a lack of measurement results in literature on the deviation behaviour of grey / white matter in different brain regions. Besides, treating ϵ in different brain regions as different variables also significantly increases the computational complexity of sensitivity analysis. Therefore, this work adopts this simplification and uses a single variable to represent the sound speed deviation. The sensitivity to all other acoustic parameters, such as attenuation coefficients and densities, are not considered and will be investigated in the future work.

The ultrasound propagation model used in this work is generalized based on literatures[6,7]. A phased array transducer with M elements is placed on the top of the grey matter, as is shown in Fig. 1 (a)[16]. The array may not be flat due to the structure of brain tissue surface. Each element m can generate a continuous ultrasonic wave at frequency f with amplitude A_m and phase ϕ_m. Then any brain tissue region G will be exposed to the stimulation of a sine wave $p(G, \epsilon, t) = [\boldsymbol{h}(G, \epsilon)]^H \boldsymbol{w} e^{j(2\pi f t - \frac{\pi}{2})}$, where $\boldsymbol{w}$ is the beamforming vector, $\boldsymbol{h}(G, \epsilon)$ is the propagation vector, and $[\cdot]^H$ denotes the conjugate transpose operation. A detailed explanation is included in the Supplementary Information. The total transducer array power is assumed to be limited, i.e., $||\boldsymbol{w}||_2^2 = P$, where P represents a scaling of the total transducer array power. The average ultrasound intensity $I(G, \epsilon)$ is defined as[6,11,24]

$$I(G,\epsilon) \approx \frac{[\boldsymbol{w}]^H \boldsymbol{h}(G,\epsilon)[\boldsymbol{h}(G,\epsilon)]^H \boldsymbol{w}}{2\rho(G)c(G)}, \tag{2}$$

where $\rho(G)$ represents the medium density at point G.

Robust optimal resolution beamforming

It has been shown in previous works that the neuronal activation can be determined by ultrasound intensity thresholds, while the neuromodulation resolution can be evaluated based on OTAA given that the target region is successfully activated[7]. When the ultrasound intensity in the target region is equal to the neuron activation intensity threshold, neurons in an off-target region can experience off-target neuromodulation effects if the ratio

between ultrasound intensity and the activation threshold is larger than η, the activation intensity ratio between off-target and target regions[25–29]. In this situation, OTAA can be approximately measured with $S(\boldsymbol{w}, \epsilon)$, i.e.,

$$S(\boldsymbol{w}, \epsilon) = \sum_{G \neq G^*} \chi\Big(I(G, \epsilon) - \eta I(G^*, \epsilon)\Big). \tag{3}$$

Here $\chi(\cdot)$ is a 0-1 step function indicating whether neurons at G are activated according to the neuron activation model. The target region is denoted by G^*. The area is equivalently represented by the number of brain regions in (3).

The OTAA-based neuromodulation resolution is generally determined by the beamforming $\boldsymbol{w}$ of phased array transducer[7], and the optimization of $\boldsymbol{w}$ relies on the knowledge of propagation $\boldsymbol{h}(G, \epsilon)$. As the exact value of $\boldsymbol{h}(G, \epsilon)$, $c(G)$ or ϵ cannot be measured *in vivo*, the beamforming coefficients can suffer from inaccuracy and degrade the neuromodulation resolution[12]. A preferable solution to this sensitivity issue is the design of a single beam pattern that robustly leads to satisfying OTAA for all possible sound speed values. Therefore, given the sound speed model (1), the ROR beamforming method is proposed to minimize the worst-case OTAA $S(\boldsymbol{w}, \epsilon)$ for any values of $\epsilon \in [\epsilon_{min}, \epsilon_{max}]$[30]. The method can be formulated as a min-max optimization problem,

$$\min_{\boldsymbol{w}} \quad \max_{\epsilon} \; S(\boldsymbol{w}, \epsilon), \;\; ||\boldsymbol{w}||_2^2 = P, \;\; \epsilon_{min} \leq \epsilon \leq \epsilon_{max}. \tag{4}$$

As this problem is non-convex with respect to $\boldsymbol{w}$, it is of significant challenge to find a solution that converges to the global optimal solution[31]. Instead, a sub-optimal solution to this formulation can be achieved with an iterative potential reduction algorithm[31–33]. A detailed introduction of the algorithm used is included in the Supplementary Information.

Estimation of propagation properties

According to the Supplementary Information, the calculation of $\boldsymbol{w}$ requires the knowledge of $\boldsymbol{h}(G, \epsilon)$ and its gradient, which can be complex to acquire with arbitrary potential values of ϵ either in experiments or simulations. The solution is to infer $\boldsymbol{h}(G, \epsilon)$ for any ϵ based on measurements / simulations at a few reference values ϵ_r and ESM. Since $\boldsymbol{h}(G, \epsilon)$ represents a linear superposition of incident waves and reflected waves in an approximately linear environment, ESM can be used to separately model these waves that are transmitted / reflected from each direction to the brain region of interest[34]. ESM assumes the reflected sound field as equivalently generated by *virtual* sound sources on the other side of the reflective boundary[35,36] (i.e., the inner skull surface in this work), which can be applied to non-flat reflection surfaces and non-plane waves that are challenging to model analytically[37]. The mathematical derivation of $\boldsymbol{h}(G, \epsilon)$ using ESM is introduced in the Supplementary Information.

Numerical evaluation

Simulation setups

This work numerically evaluates the accuracy of propagation property estimation and the sensitivity of OTAA with respect to the brain tissue sound speed deviation ϵ. Since both propagation property estimation and beamforming optimization rely on reference measurements given different values of ϵ_r, two selections of ϵ_r are evaluated in this section. The first selection is represented by ESM-1, which only use 1 measurement at $\epsilon_r = 0$. ROR beamforming based on ESM-1 is referred to as ROR-1. In practical scenario, this method can cater to the situation in which one phantom measurement is used for beamforming design, as conducting multiple phantom experiments with small sound speed variation can be difficult due to cost and complexity. The second selection is denoted by ESM-3, using 3 measurements at $\epsilon = 0$, ϵ_{min} and ϵ_{max}. ROR beamforming based on ESM-3 is referred to as ROR-3. This configuration can be used by simulation-based propagation measurement, and it is expected that the result can be improved with more reference sound speed values evaluated. Other simulation parameters are listed in the Supplementary Information.

Estimation accuracy of propagation properties

Fig. 4 (a)-(c) evaluates the estimation accuracy of propagation properties using ESM-1 and ESM-3. Given a selected pair of transducer array element m and grid point G in the brain tissue region, the change of the propagation $h_m(G, \epsilon)$ with respect to ϵ is simulated using k-wave and estimated using ESM-1 and ESM-3. Fig. 4 (a) illustrates the amplitudes of both simulated and estimated propagation, $|h_m(G, \epsilon)|$. The black curve represents the simulated propagation. The red curve denotes the estimation with ESM-1, and the blue curve denotes the estimation with ESM-3. The x-axis denotes the sound speed deviation ϵ ranging from -1% to 1%. It can be concluded based on Fig. 4 (a) that the amplitude change in propagation is sensitive to ϵ, as 1% deviation can result in a halved amplitude. Such a phenomenon is likely caused by the complicated pattern of intracranial standing waves, as the local maximum and minimum of standing waves can move if the sound speed changes. Although neither ESM-1 nor ESM-3 estimation can perfectly fit the simulated propagation, ESM-3 can provide a better estimation than ESM-1 in amplitudes by utilizing more reference measurements.

Fig. 4 (b) evaluates the propagation phase shift for the same pair of transducer element and grid point. The phase shift is also sensitive to the sound speed deviation, linearly increasing with ϵ in a small range and diverging from linearity when ϵ is large. Both ESM-1 and ESM-3 approximate the linear phase shift change well. However, only ESM-3 can estimate the non-linear phase shift change.

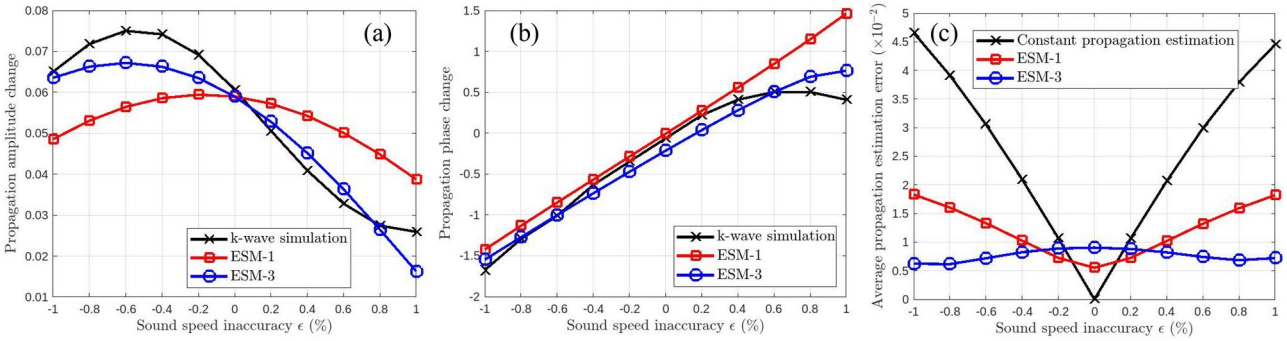

Fig. 4. (**a**) The comparison between the simulated amplitude change in propagation using k-wave and the estimation using ESM. (**b**) The comparison between the simulated phase shift in propagation using k-wave and the estimation using ESM. (**c**) The average propagation estimation error using ESM with respect to the k-wave propagation simulation.

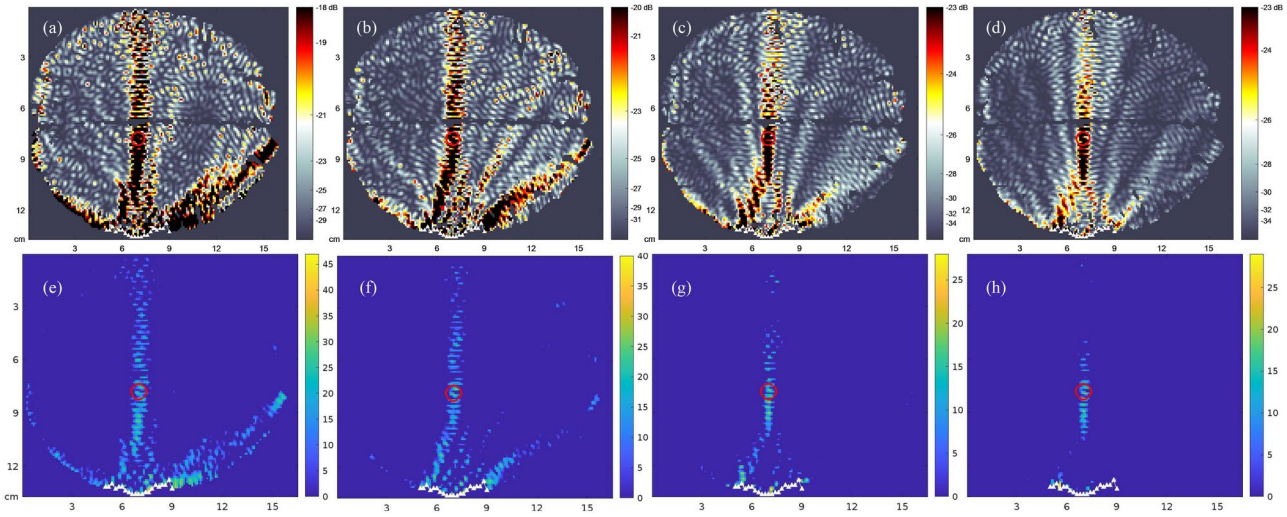

Fig. 5. The pressure-based intensity beam pattern (top) and the off-target activation area (bottom) of all beamforming methods. The maximal OTAA of each method is achieved with the corresponding ϵ value selected. (**a**) and (**e**): Conjugate beamforming; (**b**) and (**f**): COR; (**c**) and (**g**): ROR-1; (**d**) and (**h**): ROR-3.

While Fig. 4 (a)-(b) only evaluates the propagation from a single element to one brain region, Fig. 4 (c) focuses on the mean estimation accuracy for all transducer elements and brain regions. The mean absolute value of estimation errors of each method, i.e., the mean of $|\tilde{\boldsymbol{H}}_m(\epsilon) - \boldsymbol{H}_m(\epsilon)|$ for all brain regions and transducer elements, is compared. Here the black curve assumes constant propagation properties, i.e., the propagation does not change with ϵ and can be calculated with $\epsilon = 0$. This is the assumption adopted by benchmark beamforming methods in this work. Although the error is close to 0 when ϵ is close to 0, the error significantly increases for larger $|\epsilon|$. Instead, ESM-1 and ESM-3 can significantly reduce the estimation error for large $|\epsilon|$, at the expense of the estimation error for ϵ close to 0. When $\epsilon = 0$, the gap between the black curve and the red curve represents the propagation effect that cannot be accurately modeled with ESM, including the weak refractions in brain tissues, the mismatch between the wave equation solution and the ray-tracing model, and so on. On the other hand, the gap between the blue curve and the red curve at $\epsilon = 0$ represents the expense for minimizing the estimation error at other reference values ϵ_r. For sensitivity reduction and robust beamforming, the *worst-case* performance usually has the most impact, which implies ESM-3 has the best propagation estimation performance.

Sensitivity of OTAA

Fig. 5 and 6 evaluate the sensitivity of the neuromodulation resolution, measured by OTAA, to ϵ with different beamforming methods. Fig. 5 illustrates the beam patterns corresponding to the worst-case OTAA with different beamforming algorithms (Conjugate beamforming, COR, ROR-1, and ROR-3) in subfigures on the top, depicted by the spatial distribution of intensity. Subfigures at the bottom show the corresponding off-target neuron spiking map, while the dark blue areas represent regions that are not activated by ultrasound stimulation. Different beamforming methods can achieve their own worst-case OTAAs at different values of ϵ. The center of the red circle in each subfigure represents the target point. The phased array transducer elements are represented

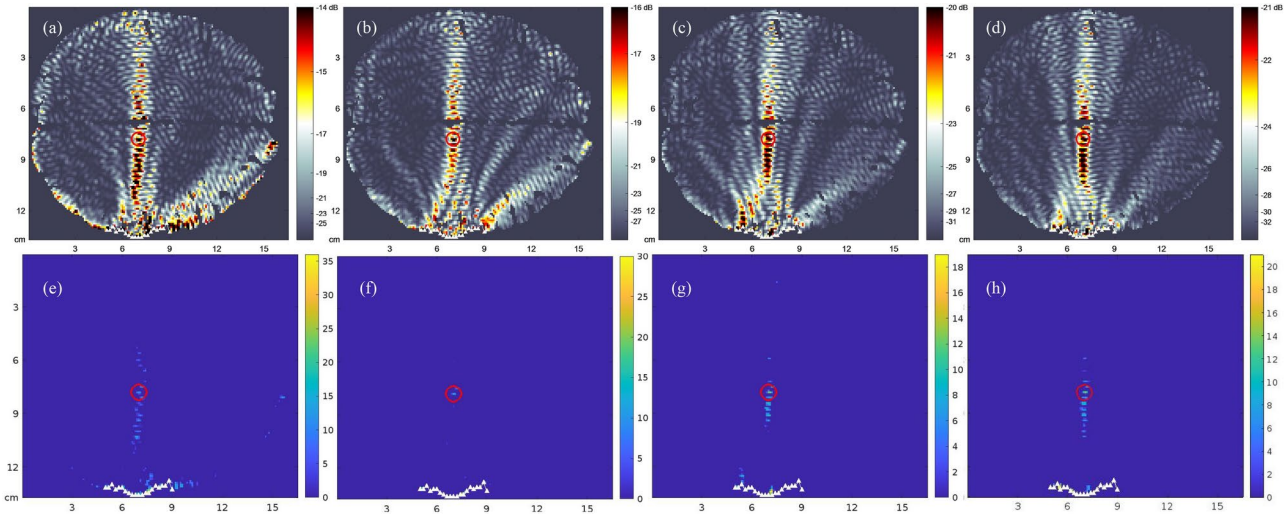

Fig. 6. The pressure-based intensity beam pattern (top) and the off-target activation area (bottom) of all beamforming methods. The minimal OTAA of each method is achieved with the corresponding ϵ value selected. (**a**) and (**e**): Conjugate beamforming; (**b**) and (**f**): COR; (**c**) and (**g**): ROR-1; (**d**) and (**h**): ROR-3.

by the white triangles. Similarly, Fig. 6 illustrates the beam patterns and off-target activation area corresponding to the minimal OTAAs with the same arrangement of subfigures.

Fig. 6 (f) shows that COR can minimize OTAA and achieve the best neuromodulation resolution compared to all other methods. Conjugate beamforming method does not focus on the neuromodulation resolution and only maximizes the target intensity. Compared to the best-case OTAA of COR, the best-case OTAAs of ROR-1 and ROR-3 have some degradation, as these two methods have focused on the robustness of neuromodulation at the expense of best-case performances. In an extreme scenario where $\epsilon_{min} = \epsilon_{max} = 0$, ROR-1 and ROR-3 are supposed to have the same OTAAs as COR.

The sensitivity of OTAA to sound speed deviation can be evaluated with the comparison between minimal and maximal OTAAs. It can be obviously concluded from Fig. 5 and 6 that OTAAs of benchmark methods are very sensitive to sound speed deviation. The worst-case OTAA of conjugate beamforming is about 8.76 times the best-case OTAA while the sound speed only changes about 1%. Similarly, COR can almost eliminate OTAA when ϵ is close to 0, but the performance significantly degrades in the worst-case scenario. Compared to benchmarks, ROR-1 and ROR-3 beamforming methods are more robust to sound speed deviations. The gaps between worst-case and best-case OTAAs of ROR-1 and ROR-3 are much smaller than the gaps of benchmark methods. ROR-3 has the minimal worst-case OTAA among all methods by focusing the majority of energy around the target point even in the worst-case, which implies that the sensitivity issue is successfully solved. Compared to ROR-1, ROR-3 further improves the neuromodulation resolution by having a better estimation of the propagation $\boldsymbol{h}(G, \epsilon)$, as is shown in Fig. 4.

Fig. 7 evaluates the sensitivity of OTAA of all beamforming methods with respect to sampled ϵ values in the whole feasible range $[\epsilon_{min}, \epsilon_{max}]$. The simulation setup is the same as in Fig. 5 and 6. To reduce the computational complexity, here we evaluate OTAA using its approximation $S(\boldsymbol{w}, \epsilon)$. The *x*-axis denotes the percentage deviation ϵ and the *y*-axis denotes OTAA. The dashed black curve denotes the conjugate benchmark. The solid black curve denotes the COR benchmark. The solid red curve denotes ROR-1, while the solid blue curve denotes ROR-3. It can be observed that the OTAA of benchmark methods significantly increases when the sound speed deviation is far from 0, and usually the maximal OTAAs of benchmark methods are achieved when $\epsilon = \epsilon_{min}$ or ϵ_{max}. However, the proposed beamforming method, especially ROR-3, almost has a flat OTAA curve with respect to sound speed deviation, demonstrating that the sensitivity issue is addressed. The robustness of ROR-3 is guaranteed at the expense of neuromodulation resolution at $\epsilon \to 0$ compared to COR and ROR-1.

Impact of target distance

Fig. 8 evaluates the worst-case OTAAs with respect to the distances between target points and the transducer to assess whether the sensitivity can be reduced for other potential target regions. To reduce the computational complexity, here we evaluate OTAA using its approximation $S(\boldsymbol{w}, \epsilon)$. It is assumed that all potential target regions are located along the axis of the phased array transducer. The solid black curve denotes the COR benchmark. The solid red curve denotes ROR-1, while the solid blue curve denotes ROR-3. The *x*-axis of the figure denotes the distance between the target brain region and the phased array, and the *y*-axis denotes worst-case OTAA. By comparing different methods, it can be concluded that ROR-1 and ROR-3 beamforming methods can generally outperform the benchmark methods for almost all target regions. Compared to the conjugate benchmark which is not plotted, on average ROR-1 can reduce worst-case OTAA by around 64.1%. Compared to COR, the average reduction of worst-case OTAA by ROR-1 is about 34.5%. ROR-3 could further reduce 60.5% OTAA compared to COR on average, and reduce 78.0% on average and up to 90.0% OTAA compared to the conjugate

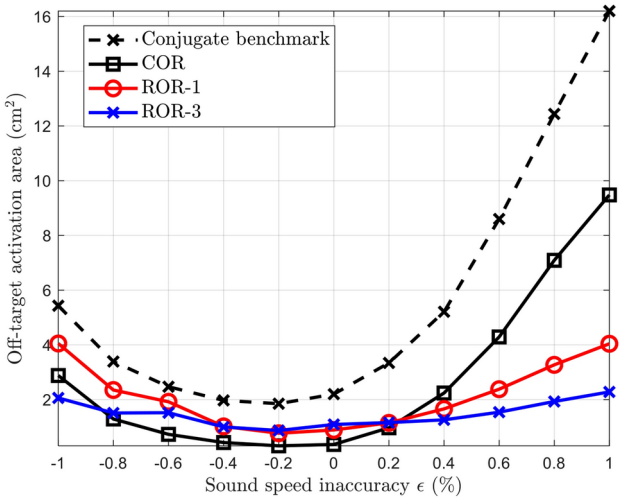

Fig. 7. Sensitivity of OTAA to brain tissue sound speed inaccuracy ϵ with different beamforming algorithms.

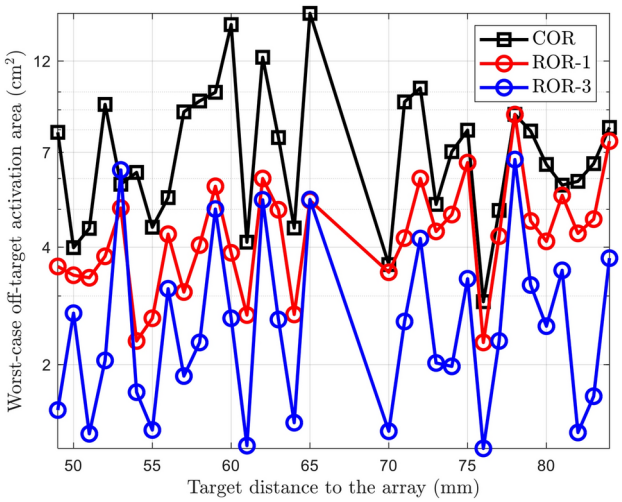

Fig. 8. Worst-case OTAA of different beamforming algorithms with respect to target locations. The feasibility of ROR for most target points near the brain center is validated. The oscillation of OTAA curves shows the evidence that the mechanism of the sensitivity is related to standing waves.

benchmark. These results show that the proposed beamforming schemes can successfully address the sensitivity issue. In some rare cases, the performances of proposed methods can be worse than benchmarks, due to the errors involved in the estimation of propagation properties. Besides, although ROR-3 generally outperforms ROR-1, in real-world applications, the selection of beamforming schemes depends on the propagation measurement setups, and a trade-off exists between the resolution and the complexity.

Obviously in Fig. 8, OTAA curves oscillate drastically with the change of target distances to the phased array. It can be inferred from such a pattern and the phenomenon in Fig. 7 that the mechanism of OTAA sensitivity is probably related to intracranial standing waves, which are generated by the reflective environment inside the skull and visualized in the previous beam pattern results. For comparison, intuitively the sensitivity issue in homogeneous medium without reflections and standing waves should not be as significant.

Discussion and conclusion

This work analyzes the sensitivity of the intracranial neuromodulation resolution, defined by OTAA, to the sound speeds of brain tissues with different beamforming methods, and a robust beamforming scheme, ROR, is proposed to minimize the worst-case OTAA and robustly stimulate the target brain region with high resolution. Simulations show that the ultrasound propagation in brain tissues is sensitive to the sound speed deviation, and such dependence can be approximately estimated based on ESM and reference measurements. The ROR beamforming method can also significantly reduce the sensitivity of OTAA to the sound speed deviation and maintain high neuromodulation resolution even in the worst case, whereas benchmarks methods all suffer

from the sensitivity issue. Simulations with different target locations show that the worst-case OTAA drastically oscillates with respect to the distance between the target brain region and the phased array transducer.

It can be inferred that the standing wave can be a potential cause of the OTAA sensitivity. In the intracranial setup, the standing wave is mainly generated by the superposition of incident waves and the reflected waves from the inner surface of the skull, which can also have neuromodulation effects[4]. According to the example propagation in literature[6,7], such superposition can happen in 0.3 ms since the start of the stimulation for a human subject, which is shorter than most pulse durations for human stimulation in the literature[2,21,26,38]. Therefore, it might be challenging to eliminate the standing wave effect completely. From this perspective, as the ROR beamforming can successfully address the sensitivity issue for continuous-wave or even long-pulse stimulation, this proposed method provides more options of transducer parameters to be feasible in ultrasound neuromodulation.

Most previous research has utilized single-element curved transducers to focus the ultrasound to the target brain region, which cannot counter the attenuation and phase shift along the propagation path. Acoustic lenses can be built to match the propagation channel for a determined target point but have little flexibility[10,39]. In contrast, a phased array transducer supported by beamforming algorithms[7,11,40–42] can flexibly focus the energy to any locations in brain tissues with high neuromodulation resolution[7,11,40,41]. Furthermore, when the size is limited, the phased array transducer can even be implanted inside the skull or on the surface of brain tissues to reduce the aberration further and increase the energy efficiency[16,43]. Therefore, the main focus of this work is to pursue high neuromodulation resolution in the intracranial LIFU stimulation by utilizing implanted phased array transducers and beamforming techniques[44,45].

To accurately focus the ultrasound energy on the targeted brain tissue, the attenuation and phase shift information during propagation, i.e., the propagation channel, is necessary. According to literature[8], currently the most accurate method to measure the propagation inside the brain tissue is to implant a hydrophone into the brain of the patient *in vivo*, which is highly invasive and inflexible. A non-invasive alternative is to record the wave propagation resulted from the collapse of a cavitation bubble, which is generated at the target using an ultrasound transducer[46]. Magnetic resonance acoustic radiation force imaging (MR-ARFI) is also a tool for measuring the propagation channel *in vivo*[47]. However, it can be very time-consuming to acquire propagation information for all brain regions with these methods, which is necessary for achieving high neuromodulation resolution[6,8]. Instead, simulations and phantom experiments can serve as non-invasive alternatives to acquire such propagation information[8,48]. To further reduce the complexity of simulation, ESM-1 and ROR-1 can be used to improve robustness of beamforming compared to traditional methods without requiring any additional simulation or measurement.

This work only evaluates the sensitivity of OTAA to the brain tissue sound speed. Other acoustic parameters of brain tissues, like the attenuation, can also influence the ultrasound propagation[49], and a similar model can be used to infer the propagation and analyze the sensitivity as is shown in the Supplementary Information. Besides, there are many other sources of uncertainty in practical LIFU systems that could affect targeting and neuromodulation effects, such as transducer properties, skull and tissue geometry, tissue temperature change, etc. The proposed beamforming framework may not be able to take all these factors into account by itself due to the high complexity. However, it can potentially be combined with closed-loop feedback techniques to provide better targeting, e.g., propagation estimation by ESM can be refined with real-time measurements.

In addition to OTAA, safety constraints also need to be considered in clinical applications of LIFU neuromodulation technology. Two major types of LIFU stimulation effects that may raise safety concerns are heating and cavitation[50]. Two metrics have been generally used in literature to quantify heating effect of ultrasound stimulation: thermal index (TI) and spatial-peak temporal average intensity (I_{spta}), which are defined in the following formulas,

$$\mathrm{TI}(G) = \frac{W_p}{W_{deg}},\ I_{spta}(G) \approx I(G) \times T \times \mathrm{DC}. \tag{5}$$

Here W_p represents the acoustic output power; W_{deg} is the approximate power needed for 1 $^\circ C$ temperature increase; T is the stimulation duration and DC represents the duty cycle (100% for continuous wave stimulation). TI for different tissues (e.g., soft tissue, bone, cranial bone) and different beam patterns can be calculated with different definition of W_p and W_{deg} in literature[51,52]. E.g., with the array configuration and brain stimulation pattern specified in this work, W_p and W_{deg} need to be defined as[52]

$$W_p = \max_G\ \min\{W_o,\ I(G) \times 1\mathrm{cm}^2\},\ W_{deg} = \frac{210\mathrm{mW}}{f/1\mathrm{MHz}}, \tag{6}$$

where $W_o \propto ||\boldsymbol{w}||_2^2$ is the total transducer power. On the other hand, the probability of cavitation may be generally characterized with mechanical index (MI), although there is still debate on the applicability of such modeling with all ultrasound parameters[51,53]. MI in the current problem can be defined as[52]

$$\mathrm{MI} = \frac{\max_G |p(G,t)|}{\sqrt{f}}. \tag{7}$$

There has been guidelines requiring $I_{spta} \leq 720$ mW / cm^2, TI ≤ 6 and MI ≤ 1.9 for safety[53], which needs to be comprehensively integrated in beam focusing design. The beam focusing optimization problem can use these metrics and thresholds as constraints in optimization or combine them into the objective function as weighted regularization to meet requirements in both OTAA and these safety aspects. A preliminary framework

to integrate safety constraints into the proposed beam focusing method is presented in the Supplementary Information.

This work has made some simplification assumptions to better focus on the robust beamforming framework which could be relaxed and examined in future works. The estimation of propagation properties based on ESM assumes weak refraction and ray-like propagation in the region of interest[54–56], implying that it can only be applied to model the propagation in weakly heterogeneous media like brain tissues[57]. For transcranial stimulation, due to the large sound speed difference between brain tissue and skull, it is necessary to consider refraction on the skull surface and the ray-like simplification needs to be modified. However, the proposed beamforming method, ROR, can also be applied to counter the acoustic parameter deviation of other tissues like the skull, as long as the knowledge of the simulated / experimentally measured propagation function $\boldsymbol{h}(G, \epsilon)$ for a group of sampled ϵ is available.

Due to a lack of measurement results on the deviation behaviour of grey / white matter in different brain regions, this work only considers a uniform deviation ratio of sound speed values in all regions for simplification and computational complexity reduction[12,13]. This assumption might not reflect the actual deviation pattern, and such discrepancy could result in inaccuracy in ESM propagation estimation. However, correct deviation models are necessary for quantification of such inaccuracy and mitigation in propagation estimation. Sound speed measurements in brain tissues, especially for the same type of tissue in different brain regions, could be conducted in the future to enable tissue-specific / location-specific deviation modeling. If the sound speed deviation ratio $\boldsymbol{\epsilon} = [\epsilon_g, \epsilon_w]$ has different values ϵ_g and ϵ_w for grey and white matter, the min-max optimization problem (4) needs to optimize the beam pattern considering all potential combinations of ϵ_g and ϵ_w, and the wave propagation model of ESM in the Supplementary Information needs to consider ϵ_g and ϵ_w separately as well. A more detailed explanation is included in the Supplementary Information. In addition, the real deviation model can also be a noisy perturbation of sound speed values, meaning different locations will have different random sound speed variation values[12]. In this case, the mean deviation value may be used for propagation approximation and calibration with actual sound field. Future works will test different sound speed deviation models and validate the performance of the proposed beam focusing scheme with more generalized setups.

In addition, this work has also assumed continuous wave stimulation to simplify modeling and significantly reduce computational complexity. Pulsed waves have been more commonly used in human neuromodulation studies[21], and using continuous wave stimulation for approximation may lead to inaccuracy in beam pattern and neuron responses. The beam pattern approximation accuracy mainly depends on the pulse duration. As previous analysis has shown that intracranial sound field may become stable after 0.5 to 0.7 ms stimulation[7], shorter pulse duration can lead to dynamic sound field and approximation inaccuracy. The neuron activation patterns with continuous / pulsed wave stimulation are also different[17]. Besides, the thermal effect of continuous wave is also more significant. Therefore, to accurately show the stimulation performance of all pulsed-wave setups, future work needs to consider time-aware intensity for beam focusing design[7], and quantify the difference of pulsed wave and continuous wave in beam focusing pattern, neuron behaviors, and thermal effects (e.g., using TI).

This work mainly focuses on the ultrasound focusing design and has only considered a simplified model of neuronal responses to ultrasound stimulation. Factors including the type of neuron, the type of neuromodulation effects (excitatory / inhibitory, etc.), and the brain circuit effect / neural network effect have all been shown to influence the neuromodulation phenomena in literature, and can be integrated into the analysis in future investigation[17,28,58–61]. For example, previous research[59] has demonstrated that the activation of regular spiking neurons significantly increase with pulse repetition frequency (PRF), whereas fast spiking neurons have homogeneous spike rate that does not change with PRF. Similarly, hippocampal pyramidal neurons and neighboring inhibitory basket cells have opposite neuromodulation effects during the same ultrasound stimulation[62], and the same stimulation protocol can result in different neuron behavior in ventral tegmental area GABAergic and dopaminergic cells as well[60]. Such cell-type-specific stimulation has shown potentials to be used for precise psychiatric disorder therapy, and its combination with optimized spatial focusing precision will be more promising by further reducing side effects during stimulation. Integrating pulse parameters into the proposed method requires generating and processing time-varying sound fields when pulse duration is small, leading to increasing computational complexity that could be further optimized.

The future work of this research can be focused on extending the analysis to 3-D environments and validating the proposed ROR beamforming method in phantom experiments[63]. To validate the proposed beamforming method in phantom experiments, a skull phantom could be built with different filling media for ultrasound stimulation evaluation. Transducer elements could be attached to the inner surface of the skull phantom for intracranial stimulation, and a hydrophone could be placed in different places inside filling media to measure the propagation from transducer. Given the propagation measurements in a reference filling medium, the range of acoustic parameters of all filling media, and the map of skull, the proposed ROR beamforming strategy can be used to design a focusing beam applicable to all filling media for ultrasound focusing sensitivity analysis. The optimized beam parameters can be used to drive transducer elements, and a hydrophone measurement of focused beam pattern in filling media could validate the robustness of the optimized beam based on our proposed method. The stimulation effect on actual neurons, however, need to be evaluated in further *in vivo* experiments. Besides, validating the effectiveness of the proposed methods in transcranial LIFU neuromodulation numerically / experimentally can be another direction to explore.

Data availability

The brain model dataset used in the current study is available in BrainWeb: Simulated Brain Database, https://brainweb.bic.mni.mcgill.ca/.

Received: 27 October 2024; Accepted: 20 March 2025

Published online: 02 April 2025

References

1. Zhang, D. et al. Antidepressant-like effect of low-intensity transcranial ultrasound stimulation. *IEEE Transactions on Biomedical Engineering* **66**, 411–420 (2018).
2. Lee, W. et al. Image-guided transcranial focused ultrasound stimulates human primary somatosensory cortex. *Scientific reports* **5**, 1–10 (2015).
3. Aurup, C., Kamimura, H. A. & Konofagou, E. E. High-resolution focused ultrasound neuromodulation induces limb-specific motor responses in mice in vivo. *Ultrasound in Medicine & Biology* **47**, 998–1013 (2021).
4. Menz, M. D. et al. Radiation force as a physical mechanism for ultrasonic neurostimulation of the ex vivo retina. *Journal of Neuroscience* **39**, 6251–6264 (2019).
5. di Biase, L., Falato, E. & Di Lazzaro, V. Transcranial focused ultrasound (tfus) and transcranial unfocused ultrasound (tus) neuromodulation: from theoretical principles to stimulation practices. *Frontiers in neurology* **10**, 549 (2019).
6. Fan, B. *Ultrasound Beamforming with High Neuromodulation Resolution and Robustness Against Inaccurate Brain Tissue Sound Speed*. Ph.D. thesis, Rice University (2021).
7. Fan, B. et al. Computational modeling and minimization of unintended neuronal excitation in a lifu stimulation. *Scientific reports* **13**, 13403 (2023).
8. Kyriakou, A. et al. A review of numerical and experimental compensation techniques for skull-induced phase aberrations in transcranial focused ultrasound. *International journal of hyperthermia* **30**, 36–46 (2014).
9. Legon, W., Bansal, P., Tyshynsky, R., Ai, L. & Mueller, J. K. Transcranial focused ultrasound neuromodulation of the human primary motor cortex. *Scientific reports* **8**, 1–14 (2018).
10. Maimbourg, G., Houdouin, A., Deffieux, T., Tanter, M. & Aubry, J.-F. 3d-printed adaptive acoustic lens as a disruptive technology for transcranial ultrasound therapy using single-element transducers. *Physics in Medicine & Biology* **63**, 025026 (2018).
11. Fan, B. *et al.* Beamforming design for high-resolution low-intensity focused ultrasound neuromodulation. In *2020 IEEE International Conference on Acoustics, Speech and Signal Processing (ICASSP)*, 906–910 (2020).
12. Robertson, J., Martin, E., Cox, B. & Treeby, B. E. Sensitivity of simulated transcranial ultrasound fields to acoustic medium property maps. *Physics in Medicine & Biology* **62**, 2559 (2017).
13. Samoudi, M. A., Van Renterghem, T. & Botteldooren, D. Computational modeling of a single-element transcranial focused ultrasound transducer for subthalamic nucleus stimulation. *Journal of neural engineering* **16**, 026015 (2019).
14. Pulkkinen, A., Werner, B., Martin, E. & Hynynen, K. Numerical simulations of clinical focused ultrasound functional neurosurgery. *Physics in Medicine & Biology* **59**, 1679 (2014).
15. Mueller, J. K., Ai, L., Bansal, P. & Legon, W. Computational exploration of wave propagation and heating from transcranial focused ultrasound for neuromodulation. *Journal of neural engineering* **13**, 056002 (2016).
16. Gougheri, H. S., Dangi, A., Kothapalli, S.-R. & Kiani, M. A comprehensive study of ultrasound transducer characteristics in microscopic ultrasound neuromodulation. *IEEE transactions on biomedical circuits and systems* **13**, 835–847 (2019).
17. Lemaire, T., Neufeld, E., Kuster, N. & Micera, S. Understanding ultrasound neuromodulation using a computationally efficient and interpretable model of intramembrane cavitation. *Journal of neural engineering* **16**, 046007 (2019).
18. Cocosco, C. A., Kollokian, V., Kwan, R. K.-S., Pike, G. B. & Evans, A. C. Brainweb: Online interface to a 3d mri simulated brain database. In *NeuroImage* (Citeseer, 1997).
19. Treeby, B. E. & Cox, B. T. k-wave: Matlab toolbox for the simulation and reconstruction of photoacoustic wave fields. *Journal of biomedical optics* **15**, 021314 (2010).
20. Sarica, C. et al. Human studies of transcranial ultrasound neuromodulation: A systematic review of effectiveness and safety. *Brain stimulation* **15**, 737–746 (2022).
21. Lee, K., Park, T. Y., Lee, W. & Kim, H. A review of functional neuromodulation in humans using low-intensity transcranial focused ultrasound. *Biomedical engineering letters* **14**, 407–438 (2024).
22. Scherba, E., Hoagland, P. A. & O'Brien, W. D. Acoustic microscopy: a study of contrast in fresh tissue. *IEEE transactions on ultrasonics, ferroelectrics, and frequency control* **41**, 451–457 (1994).
23. Kremkau, F. W., Barnes, R. W. & McGraw, C. P. Ultrasonic attenuation and propagation speed in normal human brain. *The Journal of the Acoustical Society of America* **70**, 29–38 (1981).
24. Beissner, K. On the plane-wave approximation of acoustic intensity. *The Journal of the Acoustical Society of America* **71**, 1406–1411 (1982).
25. King, R. L., Brown, J. R., Newsome, W. T. & Pauly, K. B. Effective parameters for ultrasound-induced in vivo neurostimulation. *Ultrasound in medicine & biology* **39**, 312–331 (2013).
26. Lee, W. et al. Transcranial focused ultrasound stimulation of human primary visual cortex. *Scientific reports* **6**, 1–12 (2016).
27. Plaksin, M., Shoham, S. & Kimmel, E. Intramembrane cavitation as a predictive bio-piezoelectric mechanism for ultrasonic brain stimulation. *Physical review X* **4**, 011004 (2014).
28. Plaksin, M., Kimmel, E. & Shoham, S. Cell-type-selective effects of intramembrane cavitation as a unifying theoretical framework for ultrasonic neuromodulation. *Eneuro* **3** (2016).
29. Menz, M. D., Oralkan, Ö., Khuri-Yakub, P. T. & Baccus, S. A. Precise neural stimulation in the retina using focused ultrasound. *Journal of Neuroscience* **33**, 4550–4560 (2013).
30. Nongpiur, R. C. Design of minimax broadband beamformers that are robust to microphone gain, phase, and position errors. *IEEE/ACM transactions on audio, speech, and language processing* **22**, 1013–1022 (2014).
31. Razaviyayn, M. et al. Nonconvex min-max optimization: Applications, challenges, and recent theoretical advances. *IEEE Signal Processing Magazine* **37**, 55–66 (2020).
32. Nouiehed, M., Sanjabi, M., Huang, T., Lee, J. D. & Razaviyayn, M. Solving a class of non-convex min-max games using iterative first order methods. *Advances in Neural Information Processing Systems* **32**, 14934–14942 (2019).
33. Danskin, J. M. The theory of max-min, with applications. *SIAM Journal on Applied Mathematics* **14**, 641–664 (1966).
34. Bi, C.-X., Jing, W.-Q., Zhang, Y.-B. & Lin, W.-L. Reconstruction of the sound field above a reflecting plane using the equivalent source method. *Journal of Sound and Vibration* **386**, 149–162 (2017).
35. Valdivia, N. P. & Williams, E. G. Study of the comparison of the methods of equivalent sources and boundary element methods for near-field acoustic holography. *The Journal of the Acoustical Society of America* **120**, 3694–3705 (2006).
36. Too, G.-P.J. & Wang, S. M. The application of source methods in estimation of an interior sound field. *Applied acoustics* **63**, 295–310 (2002).
37. Li, J., Wang, S., Tao, Y., Dong, C. & Tang, G. A novel expression of the spherical-wave reflection coefficient at a plane interface. *Geophysical Journal International* **211**, 700–717 (2017).
38. Legon, W. et al. Transcranial focused ultrasound modulates the activity of primary somatosensory cortex in humans. *Nature neuroscience* **17**, 322–329 (2014).
39. Maimbourg, G., Houdouin, A., Deffieux, T., Tanter, M. & Aubry, J.-F. Steering capabilities of an acoustic lens for transcranial therapy: numerical and experimental studies. *IEEE Transactions on Biomedical Engineering* **67**, 27–37 (2019).
40. Liu, H.-L. et al. Design and implementation of a transmit/receive ultrasound phased array for brain applications. *IEEE transactions on ultrasonics, ferroelectrics, and frequency control* **65**, 1756–1767 (2018).

41. Pasquinelli, C. et al. Transducer modeling for accurate acoustic simulations of transcranial focused ultrasound stimulation. *Journal of neural engineering* **17**, 046010 (2020).
42. Fan, B. & Das, S. Synthetic aperture acoustic imaging with deep generative model based source distribution prior. In *2021 IEEE International Conference on Acoustics, Speech and Signal Processing (ICASSP)*, 1420–1424 (IEEE, 2021).
43. Carpentier, A. *et al.* Clinical trial of blood-brain barrier disruption by pulsed ultrasound. *Science translational medicine* **8**, 343re2–343re2 (2016).
44. Herbert, E., Pernot, M., Montaldo, G., Fink, M. & Tanter, M. Energy-based adaptive focusing of waves: application to noninvasive aberration correction of ultrasonic wavefields. *IEEE transactions on ultrasonics, ferroelectrics, and frequency control* **56**, 2388–2399 (2009).
45. Iero, D., Isernia, T. & Crocco, L. Focusing time harmonic scalar fields in non-homogenous lossy media: inverse filter vs. constrained power focusing optimization. *Applied Physics Letters* **103**, 093702 (2013).
46. Pernot, M., Montaldo, G., Tanter, M. & Fink, M. "ultrasonic stars" for time reversal focusing using induced cavitation bubbles. In *AIP Conference Proceedings*, vol. 829(1), 223–227 (American Institute of Physics, 2006).
47. Hertzberg, Y. et al. Ultrasound focusing using magnetic resonance acoustic radiation force imaging: application to ultrasound transcranial therapy. *Medical physics* **37**, 2934–2942 (2010).
48. Naor, O., Krupa, S. & Shoham, S. Ultrasonic neuromodulation. *Journal of neural engineering* **13**, 031003 (2016).
49. Rau, R., Unal, O., Schweizer, D., Vishnevskiy, V. & Goksel, O. Frequency-dependent attenuation reconstruction with an acoustic reflector. *Medical Image Analysis* **67**, 101875 (2021).
50. Radjenovic, S., Dörl, G., Gaal, M. & Beisteiner, R. Safety of clinical ultrasound neuromodulation. *Brain Sciences* **12**, 1277 (2022).
51. Nowicki, A. Safety of ultrasonic examinations; thermal and mechanical indices. *Medical Ultrasonography* **22**, 203–210 (2020).
52. Hedrick, W. & Hykes, D. An overview of thermal and mechanical acoustic output indices. *Journal of Diagnostic Medical Sonography* **9**, 228–235 (1993).
53. Blackmore, J., Shrivastava, S., Sallet, J., Butler, C. R. & Cleveland, R. O. Ultrasound neuromodulation: a review of results, mechanisms and safety. *Ultrasound in medicine & biology* **45**, 1509–1536 (2019).
54. Sanabria, S. J., Rominger, M. B. & Goksel, O. Speed-of-sound imaging based on reflector delineation. *IEEE Transactions on Biomedical Engineering* **66**, 1949–1962 (2018).
55. Rau, R., Schweizer, D., Vishnevskiy, V. & Goksel, O. Ultrasound aberration correction based on local speed-of-sound map estimation. In *2019 IEEE International Ultrasonics Symposium (IUS)*, 2003–2006 (IEEE, 2019).
56. Yuan, Y. *et al.* A modified ray tracing method for ultrasound computed tomography in breast imaging. In *2020 IEEE International Instrumentation and Measurement Technology Conference (I2MTC)*, 1–6 (IEEE, 2020).
57. Liu, S. & Manocha, D. *Sound synthesis, propagation, and rendering* (Morgan & Claypool Publishers, 2022).
58. Manuel, T. J. et al. Ultrasound neuromodulation depends on pulse repetition frequency and can modulate inhibitory effects of ttx. *Scientific Reports* **10**, 1–10 (2020).
59. Yu, K., Niu, X., Krook-Magnuson, E. & He, B. Intrinsic functional neuron-type selectivity of transcranial focused ultrasound neuromodulation. *Nature communications* **12**, 2519 (2021).
60. Murphy, K. R. & de Lecea, L. Cell type specific focused ultrasound neuromodulation in preclinical models of sleep and psychiatric disorders (2024).
61. Kamimura, H. A., Conti, A., Toschi, N. & Konofagou, E. E. Ultrasound neuromodulation: Mechanisms and the potential of multimodal stimulation for neuronal function assessment. *Frontiers in physics* **8**, 150 (2020).
62. Murphy, K. R. et al. A tool for monitoring cell type-specific focused ultrasound neuromodulation and control of chronic epilepsy. *Proceedings of the National Academy of Sciences* **119**, e2206828119 (2022).
63. Antoniou, A., Evripidou, N. & Damianou, C. Focused ultrasound heating in brain tissue/skull phantoms with 1 mhz single-element transducer. *Journal of Ultrasound* **27**, 263–274 (2024).

Acknowledgements

The authors acknowledge the McNair Medical Institute at The Robert and Janice McNair Foundation for financially supporting this research.

Author contributions

B. F. proposed methods, conducted simulations, and wrote the manuscript with the supervision of B. A. W. G., S. A. S., R. R. B., and B. A. commented on the project and reviewed the manuscript. B. A. supervised this research.

Declarations

Competing interests

The authors declare no competing interests.

Additional information

Supplementary Information The online version contains supplementary material available at https://doi.org/10.1038/s41598-025-95396-x.

Correspondence and requests for materials should be addressed to B.F.